ADVANCED MATERIALS
www.advmat.de

Monodispersed Sub-1 nm Inorganic Cluster Chains in Polymers for Solid Electrolytes with Enhanced Li-Ion Transport

Yu Cheng, Xiaowei Liu, Yaqing Guo, Guangyao Dong, Xinkuan Hu, Hong Zhang, Xidan Xiao, Qin Liu, Lin Xu, and Liqiang Mai**

The organic–inorganic interfaces can enhance Li^+ transport in composite solid-state electrolytes (CSEs) due to the strong interface interactions. However, Li^+ non-conductive areas in CSEs with inert fillers will hinder the construction of efficient Li^+ transport channels. Herein, CSEs with fully active Li^+ conductive networks are proposed to improve Li^+ transport by composing sub-1 nm inorganic cluster chains and organic polymer chains. The inorganic cluster chains are monodispersed in polymer matrix by a brief mixed-solvent strategy, their sub-1 nm diameter and ultrafine dispersion state eliminate Li^+ non-conductive areas in the interior of inert fillers and filler-agglomeration, respectively, providing rich surface areas for interface interactions. Therefore, the 3D networks connected by the monodispersed cluster chains finally construct homogeneous, large-scale, continuous Li^+ fast transport channels. Furthermore, a conjecture about 1D oriented distribution of organic polymer chains along the inorganic cluster chains is proposed to optimize Li^+ pathways. Consequently, the as-obtained CSEs possess high ionic conductivity at room temperature (0.52 mS cm^{-1}), high Li^+ transference number (0.62), and more mobile Li^+ (50.7%). The assembled $LiFePO_4$/Li cell delivers excellent stability of 1000 cycles at 0.5 C and 700 cycles at 1 C. This research provides a new strategy for enhancing Li^+ transport by efficient interfaces.

1. Introduction

Solid-state lithium batteries (SSLBs) are promising candidates for future energy storage devices due to their high safety and high energy density.[1] Among them, organic–inorganic composite solid-state electrolytes (CSEs) have attracted great attention because of their high ionic conductivity and high interface compatibility.[2] It is an effective way to create fast Li^+ transport channels at the organic–inorganic interfaces in CSEs via strong interface interactions between inorganic fillers and solid polymer electrolytes (SPEs), which is also the main mechanism of enhanced Li^+ transport in CSEs with inert inorganic fillers because of their inner Li^+ non-conductive areas.[3] However, the functional surfaces of inert inorganic fillers that play a crucial role only occupy a small fraction of the whole material region. Thus, smaller size of inert fillers will lead to less Li^+ non-conductive areas, higher specific surface areas, and more organic–inorganic interfaces for fast Li^+ transport.[4] Chen group reported that CSEs with the smallest size of ZrO_2 nanoparticles (diameter of 220 nm) exhibited the highest ionic conductivity of 1.16×10^{-3} S cm^{-1}.[5] However, smaller inorganic fillers always have higher surface energy, making them more prone to agglomeration, which prevents the berried materials from forming fast Li^+ conductive interfaces with the polymer matrix and then creates another kind of Li^+ non-conductive areas. Moreover, the agglomeration of Li^+ conductive fillers will also affect the efficient Li^+ pathways and decrease the ionic conductivity of CSEs.[6] Therefore, it is crucial to address the issue of large size and agglomeration of fillers to achieve large-scale, homogeneous, efficient interfaces and enhance Li^+ transport efficiency.

Surface modification for small-sized materials can solve the above problems simultaneously. It is reported that quantum dot inorganic fillers with enriched surface functional groups can enhance the ionic conductivity and lithium transference number of CSEs.[7] However, small-sized particles will cause discontinuity of the interfaceHence, the final Li^+ transport channels will exist as "interface-polymer-interface". Meanwhile, smaller size means shorter channels, which is not conducive to the rapid transport

Y. Cheng, X. Liu, G. Dong, X. Hu, H. Zhang, X. Xiao, Q. Liu, L. Xu, L. Mai
State Key Laboratory of Advanced Technology for Materials Synthesis and Processing
School of Materials Science and Engineering
Wuhan University of Technology
Wuhan 430070, China
E-mail: linxu@whut.edu.cn; mlq518@whut.edu.cn

Y. Guo
Hubei Longzhong Laboratory
Wuhan University of Technology (Xiangyang Demonstration Zone)
Xiangyang, Hubei 441000, China

L. Xu, L. Mai
Hainan Institute
Wuhan University of Technology
Sanya 572000, China

L. Xu, L. Mai
State Key Laboratory of Materials Processing and Die & Mould Technology
School of Materials Science and Engineering
Huazhong University of Science and Technology
Wuhan 430074, China

The ORCID identification number(s) for the author(s) of this article can be found under https://doi.org/10.1002/adma.202303226

DOI: 10.1002/adma.202303226

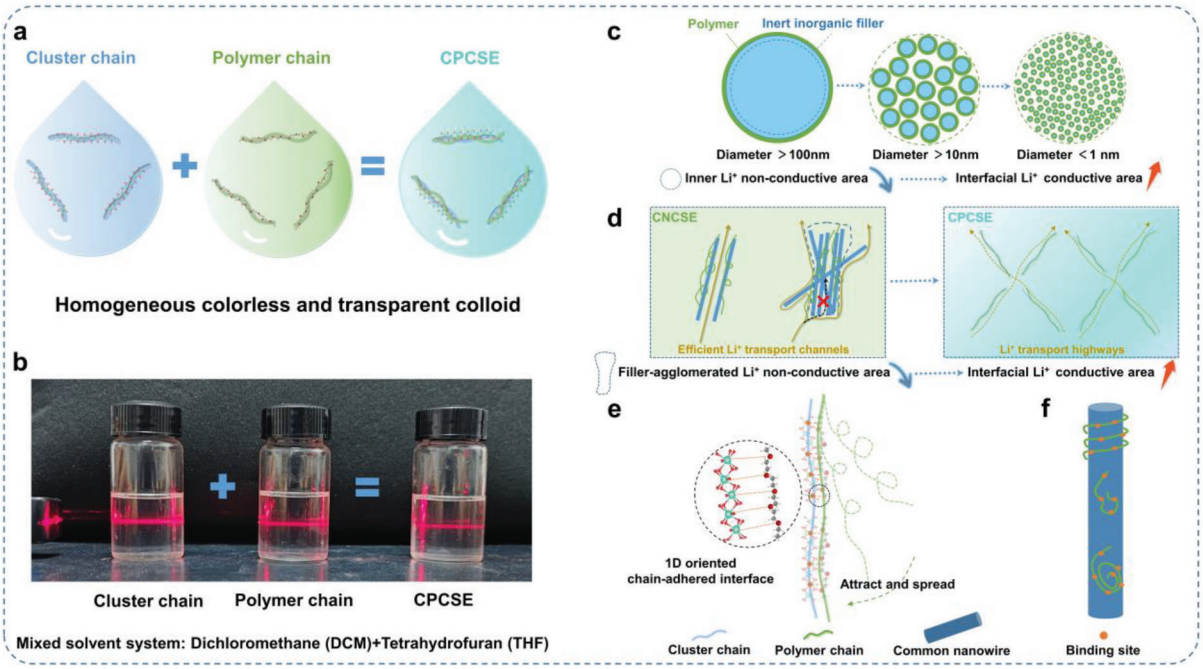

Figure 1. Organic–inorganic composite in solid-state electrolytes. a) Schematic illustration of homogeneous transparent mixtures of the cluster chain, polymer chain, and CPCSE. b) Optical images of the Tyndall effect for mixtures of the cluster chain, polymer chain, and CPCSE in the mixed-solvent system. c) Schematic illustration of interface areas in CSEs with different sizes of fillers. d) Schematic illustration of efficient Li^+ transport channels in CPCSE and CNCSE. e) Schematic illustration of the organic–inorganic composite process and 1D oriented interface in CPCSE. f) Schematic illustration of irregular organic–inorganic binding sites in CNCSE.

of Li-ions. Cui group found that 3D Li^+ conductive networks connected by 1D nanowires made the ionic conductivity of CSEs three times higher than that of CSEs with nanoparticle fillers.[8] Therefore, finding suitable small-sized 1D materials and realizing their ultrafine dispersion state in polymer matrix are essential for creating large-scale, homogeneous, continuous organic–inorganic interfaces and enhancing Li-ion transport efficiency.[9] Wang group prepared novel nanowire materials with sub-1 nm diameter and unique properties as polymer chains, which can completely disperse into colorless and transparent mixtures in weak polar and nonpolar solvents.[10] This unique characteristic is quite different from common inorganic nanowire materials, making the materials more like flexible inorganic cluster chains.[11] Therefore, this homogeneous dispersion state is favorable for application in CSEs. However, as introduced above, these inorganic cluster chain materials can only disperse well in weak polar and nonpolar solvents While the common solid polymer electrolytes (SPEs), such as poly(vinylidene fluoride-co-hexafluoropropylene) (PVDF-HFP), polyacrylonitrile (PAN), etc., prefer to dissolve in strong polar solvents, such as acetonitrile (ACN) and *N*,*N*-dimethylformamide (DMF). Therefore, the ideal organic–inorganic composite state is hard to achieve with only single component solvent. Above all, it is urgent to find an effective way to utilize this cluster chain material in CSEs.

In this work, a new type of cluster chain/polymer chain composite solid-state electrolyte (CPCSE) was fabricated for high-performance solid-state lithium batteries. The sub-1 nm inorganic cluster chains possess little inner Li^+ non-conductive areas, large aspect ratio, and rich exposed surface atoms, which provide more specific surface areas to combine with polymer chains. A compatible SPE and mixed-solvent strategy were designed to successfully achieve the monodispersion of inorganic cluster chains in the polymer matrix, which avoids the Li^+ non-conductive areas in filler-agglomeration. Hence, this novel chain-composite strategy eliminates the original defects of common inert fillers. The monodispersed cluster chains connect to form fully active Li^+ conductive networks with homogeneous, large-scale, continuous organic–inorganic interfaces, which leads to full dissociation of lithium salts and produces more mobile Li^+ at the interfaces for fast Li^+ transport. Moreover, a conjecture about the 1D-oriented distribution of organic polymer chains along the inorganic cluster chains is proposed based on the experiments and theoretical calculations. At last, a flexible composite solid-state electrolyte membrane with high ionic conductivity at room temperature (5.2×10^{-4} S cm^{-1}), large Li^+ transference number (0.62), and large distribution area of mobile Li^+ (50.7%) are obtained. The CPCSE shows excellent electrochemical stability with Li metal during long-term and rate cycling. Hence, this approach offers a novel perspective on inorganic–organic interface composites to enhance the Li-ion transport performance in CSEs.

2. Results and Discussion

The fabrication process and characteristics of CSEs are presented in **Figure 1**a. Oleylamine and oleic acid are often used as a surfactant in the synthesis of nanomaterials, which inhibits the continuous growth of hydrophilic crystal nuclei and prevents material aggregation.[12] Considering the different dispersion

characteristics of organic and inorganic materials, the mixed solvent system of tetrahydrofuran (THF) and dichloromethane (DCM) are used to achieve uniform composite of inorganic cluster chains and organic polymer chains. DCM helps to break the intermolecular forces between the oleylamine molecules and separate each single cluster chain.[13] The lower boiling point of DCM also facilitates volatilization and improves film formation. Meanwhile, THF is often used to disperse oleic acid-coated nanomaterials, and its cyclic molecules help to prevent the re-agglomeration of cluster chains.[14] Under this mixed solvent system, uniform dispersion of cluster chains is achieved to make the mixture completely colorless and transparent (Figure 1b). Additionally, the entire polarity of this solvent mixture can also uniformly dissolve the polyethylene oxide (PEO) powders and lithium salts, providing a good basis for the subsequent homogeneous composite of cluster chains and polymer chains. The homogeneous transparent state of the overall CSE mixture is not destroyed after mixing, indicating the good compatibility of this composite system. For the selection of solvents, the primary goal is to have good dispersion of inorganic cluster chains for all the solvents. The introducing of strong polar solvents will cause rapid settlement of cluster chains and disrupt their excellent dispersibility. Then, the polarity of the mixed solvent needs to be adjusted to improve the solubility of polymers and lithium salts, ensuring the stability and uniformity of the final mixture. The Tyndall effect test is taken for these three mixtures A stable laser pass through three mixtures from left to right, containing the cluster chain mixture, the polymer chain mixture, and the CPCSE mixture, respectively. The intensity and stability of the laser remain stable in these three colloids, verifying the homogeneous state of the cluster/polymer chains composite in the mixture. Even though the report about the quantum dot materials as fillers in CSEs has not observed this colorless and transparent colloid state.[7b] It is proved that the designed solid polymer electrolyte and mixed solvent show great compatibility for the dispersion of sub-1 nm inorganic cluster chains.

Figure 1c shows the interface area in CSEs with different sizes of inert fillers. The decrease of material size not only increases the specific surface areas, but also decreases the inner Li+ nonconductive areas, leading to more exposed atoms on the surface in the unit volume. Consequently, smaller size inorganic fillers facilitate to increase the organic–inorganic interfacial Li+ conductive area. Figure 1d is the schematic illustration of Li^+ transport channels in common nanowire composite solid-state electrolytes (CNCSE) and CPCSE. For common nanowires, the areas of effective Li^+ interface channels are greatly limited because of the agglomeration of nanomaterials. On the contrary, in the ideal dispersion state, the inorganic cluster chains can achieve monodispersion in the mixed solvent and uniformly composite with organic polymer chains. The excellent dispersion and chain structure with high aspect ratio greatly increase the exposed specific surfaces for the interface construction. Therefore, the monodispersed cluster chains finally connect to form the fully active Li^+ conductive networks in the polymer matrix. According to the characteristics of the cluster chains. Figure 1e proposes a possible conjecture about the composite formation process. Organic polymer chains tend to be in a flexible state in the uniform good solvent system The radial spiral twining of polymer chains on one sub-1 nm cluster chain would encounter greater steric hindrance because the length of polymer chains is far longer than the sub-1 nm diameter of cluster chains. Hence, the organic–inorganic binding sites on the cluster chain surface may prefer to present in a 1D-oriented axial distribution rather than the radical distribution. Under the shear force and the binding force during mixing, the original curled organic polymer chains would be gradually attracted and stretched on the cluster chain surface to achieve a 1D-oriented composite structure, which could provide long-range continuous chain-adhered interface channels for Li^+ transport. On the contrary, the binding sites on the relatively large-scale common nanowires mainly present irregular 3D distribution, which is difficult to construct oriented Li^+ transport channels on the surface (Figure 1f). Therefore, with the help of oleylamine and oleic acid, the cluster chains maintain a sub-1 nm diameter and high aspect ratios. In addition, small organic molecules will adhere to the surface of cluster chains, providing favorable conditions for their monodispersion in mixed solvents. Hence, the small organic molecule plays a significant role in the construction of effective organic–inorganic interfaces.

In order to realize the homogeneous organic–inorganic composite, the morphology and dispersion characteristics of cluster chains are studied. The mixture remains transparent and stable for a long time even at high concentrations. As shown in **Figure 2**a–c, the cluster chain materials tend to align into bundles at high concentrations The residual organic molecules on the surface act as surfactants to avoid the irregular agglomeration of cluster chains. Moreover, the diameter of the self-assembled bundles gradually decrease when the concentration of mixture decreases. The high-resolution TEM image is shown in Figure 2d. The diameter of the synthesized inorganic cluster chain is ≈0.95 nm. More details and the sub-1 nm diameter of cluster chains can be observed in Figure S1 (Supporting Information). Figure 2e is the scanning transmission electron microscopy (STEM) image of cluster chains on the substrate. The originally arranged cluster chains are separated, indicating the inter-molecular force between cluster chains is easily destroyed under the other external forces, which means the cluster chains have the chance to present the more uniform dispersion state under the appropriate concentration. The in situ liquid TEM was conducted to observe the morphologies of inorganic cluster chains combined with PEO in the mixed liquid, which clearly reveals the monodisperse state of inorganic cluster chains in the mixed liquid (Figure 2f). Figure 2g,h are the ultrathin section transmission electron microscope (TEM) images of CSE films to investigate the actual dispersion state of cluster chains in the CSE film. It is clear that cluster chains with sub-1 nm diameter exhibit the monodisperse state in the CSE filmwithout obvious agglomeration and entanglement, which will extremely increase the homogeneous distribution of organic–inorganic interface areas in the polymer matrix. Polymer molecules wrap on the surface of inorganic cluster chains to reduce the surface energy and the molecular force between small molecules, thereby preventing the cluster chains from re-aggregating. Therefore, each monodispersed cluster chain can be regarded as an independent and stable individual. Finally, the monodispersed cluster chains connect into a 3D structure in the polymer matrix after mixing. To certify the good dispersion state of cluster chains, ≈2.5–12.5 wt.% cluster chain materials are dispersed in the CSE mixture with mixed solvent The CSE mixtures can still maintain the completely colorless and transparent

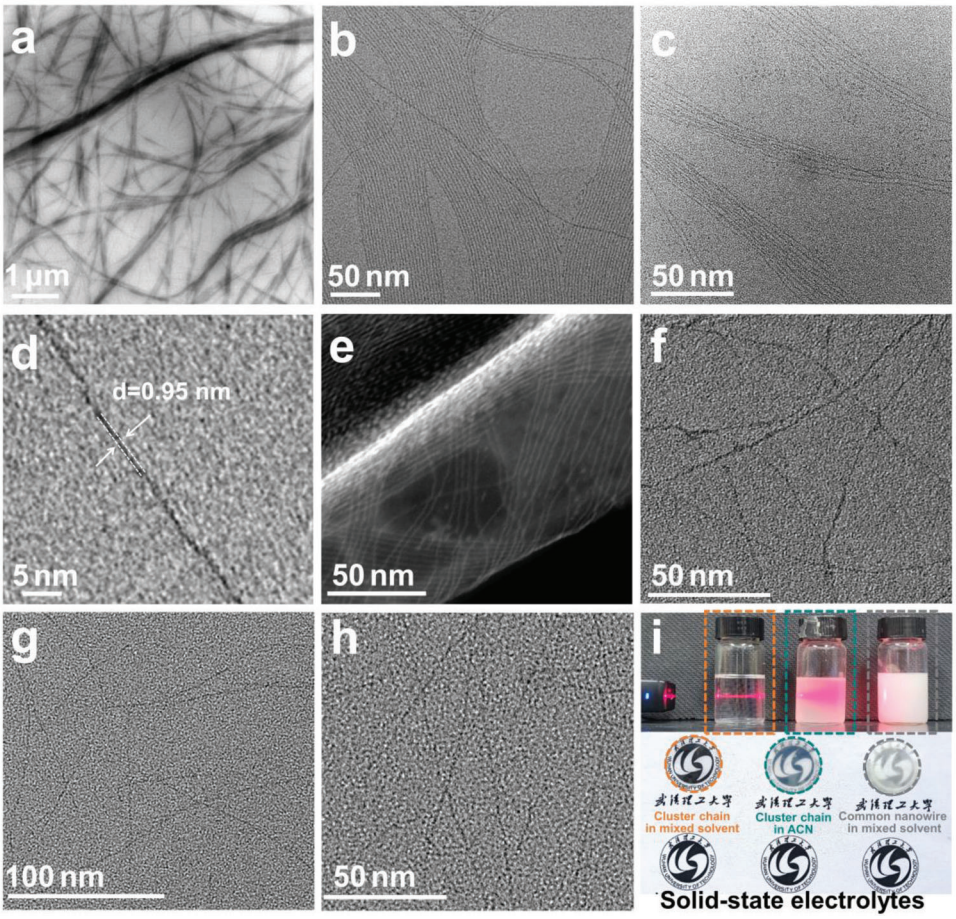

Figure 2. Morphology of cluster chain and composite solid-state electrolytes. a–c) TEM images of cluster chains under different dispersion concentrations, a,b,c) concentrations of cluster chains gradually decrease. d) TEM image of one single inorganic cluster chain with a diameter of 0.95 nm. e) STEM image of cluster chains. f) The in-situ liquid TEM image of the cluster chain/PEO/LiTFSI mixed liquid. g,h) Ultrathin section TEM images of the CPCSE film. i) Optical photographs of the Tyndall effect in CSE mixtures and CSE films, including PEO-based CSEs with cluster chain in mixed solvent (orange), cluster chain in acetonitrile (green), and common nanowire in mixed solvent (gray).

state (Figure S2, Supporting Information). The transparency of the mixture is not affected by the increased amount of inorganic cluster chains. Figure 2i contains the optical images of CSEs for different filler/solvent systems under the Tyndall effect test. It can be found that a stable laser path only occurs in the CPCSE colloid, demonstrating a homogeneous composite state of the overall components. However, in the other two nanowire/solvent systems, no stable laser appears because the cluster chains cannot realize the monodispersion in the strong polar of ACN. The large-scale common nanowire also cannot achieve the homogenous dispersion in the mixed solvent. The lower part of Figure 2i is the optical images of three different SSE films. The CPCSE film basically exhibits a completely colorless and transparent state and can clearly see the logo below. While in the second and third CSE films, the transparency gradually decreases, indicating the best uniformity of the monodispersion cluster chain system. The optical photos of the CPCSE membrane are provided in Figure S3 (Supporting Information), which show good self-supporting performance due to the enhancement of the inorganic cluster chain networks in the polymer matrix. EDS tests were performed on the CPCSE film in Figure S4 (Supporting Information). The mapping plots show a uniform distribution of the gadolinium element, which verifies the homogeneous dispersion of cluster chains. Therefore, the designed composite system perfectly solves the dispersion of inorganic filler in SPEs, which lays a favorable foundation for constructing efficient Li^+ transport channels.

The control group of large-scale common nanowires was synthesized by a similar hydrothermal method. The diameter of the nanowires was regulated by adjusting the ratio of oleylamine, oleic acid, and the reaction time. The final diameter is about 70 nm, and the length is comparable to that of cluster chains, which is about 500 nm (Figure S5, Supporting Information). The common nanowires are usually promiscuously distributed and highly prone to agglomeration, which is unfavorable to the subsequent composite with the polymer electrolyte. The XRD spectra of cluster chain materials and common nanowires are consistent with the GdOOH crystalline phase (Figure S6, Supporting Information), which is consistent with the previous report.[15] The thermogravimetric (TG) curves are shown in Figure S7, Supporting Information. About 50 wt.% organic molecules on the surface of cluster chains and common nanowires. The organic molecules

on the surface of cluster chains and common nanowires were verified by FT-IR characterization (Figure S8, Supporting Information). The results are consistent with the main characteristic peaks from the oleylamine and oleic acid molecules on the surface.[16]

To demonstrate the compatibility of the mixed solvent system with cluster chains and polymer chains in this work, several other common SPE systems are prepared for comparison. Figure S9a (Supporting Information) shows the mixture of cluster chain and PEO-based SPE in the mixed solvent, respectively, which both maintain uniform colorless and transparency state. Figure S9b (Supporting Information) are the images of the cluster chain in the mixed solvent, ACN solvent, and DMF solvent, respectively. The transparency of the mixture gradually decreases due to poor dispersibility. Other common SPE materials were applied to verify the compatibility with cluster chains (Figure S9c, Supporting Information). DMF solvent was used because the mixed solvent was less polar and could not dissolve the PVDF-HFP and PAN polymer powders. While cluster chains could not be dispersed well into the transparent mixture in this strong polar solvent. Thus, the latter two composite solid electrolyte mixtures were basically in a turbid state. Figure S9d,e (Supporting Information) are the tests of the Tyndall effect in different directions. The laser could pass through the CPCSE mixture, but could not pass through the CSE mixture with acetonitrile solvent. The results prove only PEO and the mixed solvent system used in this work are perfectly compatible with the inorganic cluster chain in the current mainstream polymer electrolyte and solvent systems. The images of the CPCSE and CNCSE mixture after 2 weeks standing are provided in Figure S10 (Supporting Information), which shows that the CPCSE mixture still keep transparent. However, the common nanowires begin to settle in the mixed liquid. These results indicate the stable dispersibility of cluster chains in the mixed solvent. CSEs of different systems are fabricated into films to test their ionic conductivity. The CPCSE shows the highest ionic conductivity of 5.2×10^{-4} S cm^{-1} at room temperature due to the homogeneous and continuous organic–inorganic interfaces (Figure S11, Supporting Information). The ionic conductivity of CSEs prepared by cluster chains and poor solvent/polymer system is even lower than that of the common nanowire system, indicating even small-size materials cannot exhibit good performance without a good dispersion situation. Even the same PEO and cluster chain system cannot be effectively composited in the incompatible solvent. On the contrary, the common nanowires/PVDF-HFP and common nanowires/PAN SSE have similar ionic conductivity with the cluster chains/PVDF-HFP and cluster chains/PAN SSE, respectively, due to the poor dispersion states. Thus, it shows that the designed mixed solvent successfully compels both cluster chains and polymer chains into a stable homogeneous mixture. The good dispersibility of inorganic additives is the key to provide effective inorganic/organic Li^+ paths and high ionic conductivity for SSEs.

In order to study the influence of inorganic filler in the CSEs, the crystallinity of the CSE films was characterized by the X-ray diffraction (XRD) test. It can be seen in **Figure 3**a that the pure polymer solid-state electrolyte (PPSE) film has two obvious peaks at 19° and 23°, which is consistent with the XRD pattern of polymer powders in Figure S12 (Supporting Information). However, as for the CNCSE film, the peak at 19° appears significantly broader and the peak intensity becomes weaker, indicating the reduction of the polymer crystallinity. While in the CPCSE film, the peak at 23° is weakened, indicating the further decrease in crystallinity. The XRD spectrum demonstrates that uniform monodispersion of cluster chains greatly destroys the crystallinity of polymer, which will be beneficial to reduce the complexation of polymer toward Li-ions and improve the Li^+ transport efficiency (Figure 3b).[17] To further test the crystallinity of the composite solid-state electrolyte film, the glass transition temperatures (T_g) of the solid-state electrolyte (SSEs) films were tested by differential scanning calorimetry (DSC). The results show that the T_g of the CNCSE film slightly decreases after the addition of common nanowire materials. However, after the introduction of cluster chains, the T_g of the CPCSE film significantly decreases to −50.51 °C. This result significantly confirms the uniform monodispersion of cluster chains can greatly reduce the crystallinity of the SSE film. Therefore, the polymer chains in the amorphous region have higher flexibility, which is conducive to compositing with cluster chains.[18] The thermogravimetric tests of the composite solid electrolyte show high thermal stability (Figure S13a, Supporting Information), which remains stable at about 350 °C. As shown in Figure S13b (Supporting Information), the weights of SSE membranes keep over 99.5% before 100 °C, which suggests that the residual solvent has been removed during the SSE fabrication process. The flatness of the solid electrolyte film is one of the important factors affecting the stability of the interface with the electrode (Figure S14, Supporting Information). The reduced crystallinity makes the films more uniform and flatter after solvent volatilization, which is conducive to close adhesion with the electrode materials. In contrast, the crystallinity of the polymer in the comparison sample is relatively high, and obvious wrinkles can be seen on the film surface. The gaps between SSE and electrodes will lead to interface failure when assembling the solid-state battery. To verify the electrochemical stability window of the SSEs, linear sweep voltammetry (LSV) tests were performed (Figure 3c), the results show the electrochemical stability windows are all improved after the addition of inorganic fillers. The electrochemical window of the CPCSE is 5.1 V, benefited by the introduction of cluster chains and Lewis acid–base interaction between cluster chains and $TFSI^-$ anions.[19] It also proves the stability of inorganic cluster chains under high voltage.

As shown in Figure 3d, the Li^+ transference number of the solid-state electrolyte was studied to verify the Li^+ transport efficiency. The CPCSE reaches the highest Li^+ transference number of 0.62 due to its homogeneous chain-adhered interface construction, which improves more interface areas to the dissociation of lithium salts. The common nanowires SSE only slightly improves the ion transference number to 0.27 due to some ineffective interfaces caused by agglomeration and large inner areas. (Figure S15, Supporting Information). The sub-1 nm size and monodispersion of cluster chains are conducive to providing more interface areas to boost the space charge layer effect, which can enhance the Li^+ transport in fully active Li^+ conductive networks.[20] The ionic conductivity of the SSEs is compared for different filler ratios (Figure S16, Supporting Information). The results of cluster chains and common nanowires show a peak at one particular ratio, mainly related to the best dispersion state of

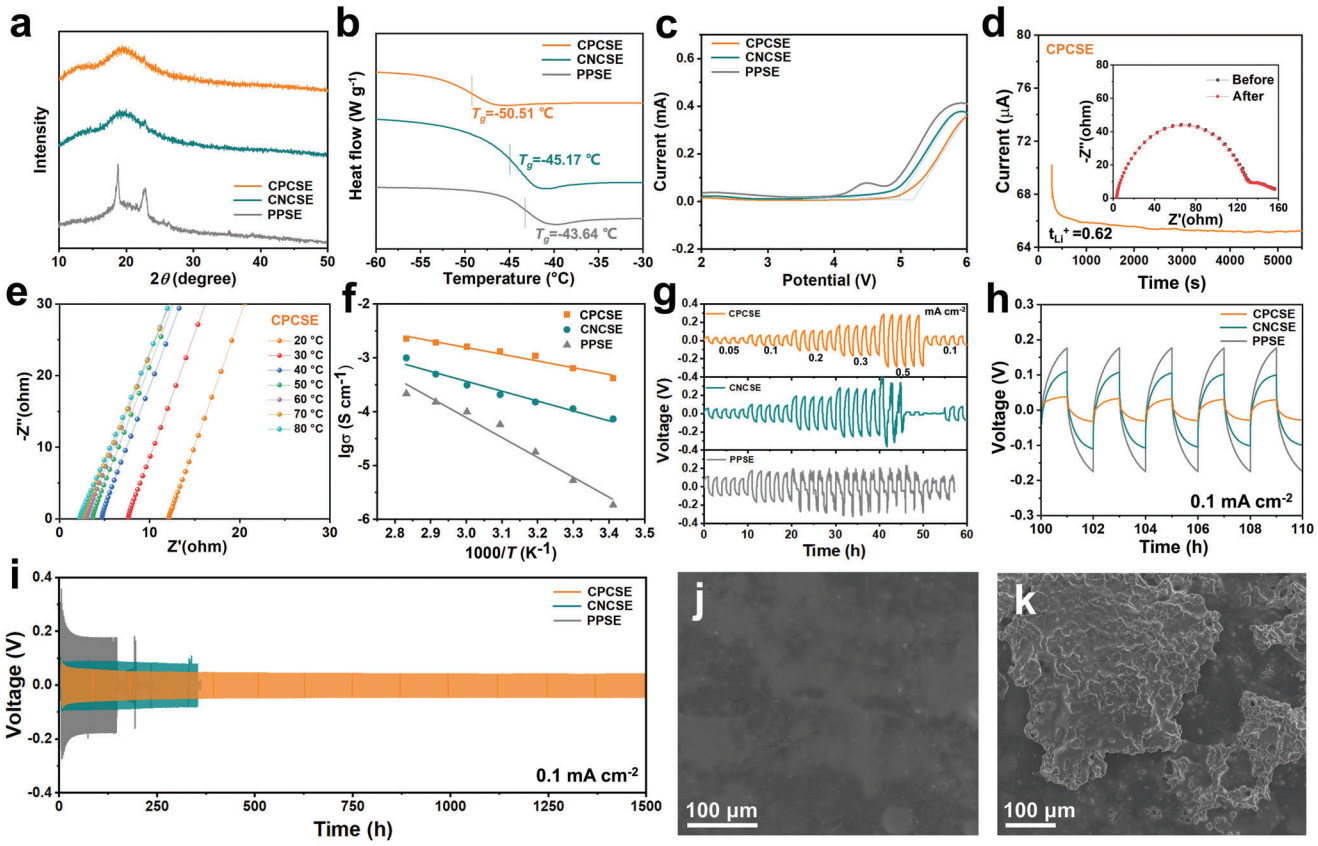

Figure 3. Crystallinity, electrochemical property, and interfacial stability of SSEs. a) XRD patterns of CPCSE, CNCSE, and PPSE. b) DSC profiles of CPCSE, CNCSE, and PPSE. c) Linear sweep voltammetry curves of CPCSE, CNCSE, and PPSE. d) Current-time curves of CPCSE Li symmetric cell, insert the corresponding EIS curves before and after polarization. e) EIS curves of CPCSE at different temperatures. f) Arrhenius plots of CPCSE, CNCSE, and PPSE at different temperatures. Galvanostatic Li plating/stripping profiles of Li/CPCSE/Li, Li/CNCSE/Li, and Li/PPSE/Li cells at g) step-increased current densities from 0.05 to 0.5 mA cm^{-2}, and 0.1 mA cm^{-2} for h) 100–110 h and i) 1500 h, respectively. SEM images of Li metal surface after j) CPCSE and k) CNCSE Li symmetric cell cycling for 300 h.

the filler and the interfacial configuration with the polymer. The ionic conductivity peak of the CNCSE shows at 10 wt.%, which is consistent with the reported inorganic filler materials. The ionic conductivity of the CPCSE reaches a peak at 2.5 wt.% due to the sub-1 nm size, proving the successful organic–inorganic interfacial construction with little cluster chain materials. The ionic conductivity of the CPCSE at different temperatures was tested (Figure 3e), and the ionic conductivity of the CPCSE reaches 1.6 × 10^{-3} S cm^{-1} at 60 °C. As for the CNCSE, the value decreases to 9.1 × 10^{-4} S cm^{-1} at 60 °C. Specifically, the ionic conductivity of PPSE at 60 °C is 0.8 × 10^{-4} S cm^{-1} (Figure S17, Supporting Information). The calculated activation energy of the CPCSE is significantly lower, which is 0.11 eV compared with 0.16 eV of CNCSE and 0.32 eV of PPSE (Figure 3f). The monodispersed cluster chain increases the contact area with the polymer, which effectively reduces the crystallinity of the polymer and constructs a continuous fully active Li^+ conductive networks. Therefore, there is an obvious increase in the transport efficiency of Li-ions in the SSEs. To demonstrate the stability of SSEs, Li–Li cycling tests were carried out at increased current densities from 0.05 to 0.5 mA cm^{-2} (0.05 to 0.5 mAh cm^{-2}). The Li–Li cell with CPCSE remains stable under the increased current. However, the short-circuiting occurs in cells with CNCSE and PPSE at high current densities, proving the homogeneous and continuous organic–inorganic interface favors electrochemical stability at high current density (Figure 3g). To further test the stability of the SSEs with lithium metal, a long cycling test of Li–Li at a current density of 0.1 mA cm^{-2} (0.1 mAh cm^{-2}) was carried out. When the cells stabilize, the Li|CPCSE|Li cell shows the lowest polarization voltage due to the homogeneous and continuous Li^+ transport channels (Figure 3h). Furthermore, the Li|CPCSE|Li cell stably cycled for 1500 h and the polarization was stable at around 40 mV (Figure 3i). While the CNCSE showed short-circuiting and polarization of 0.1 V at 400 h. The Li|PPSE|Li cell shows larger polarization, and short-circuiting occurred after 180 h. The stable lithium-SSE interface comes from the smoother SSE surface brought by the reduction of crystallinity. With the help of fully active Li^+ conductive networks, the fast lithium-ion conduction and full dissociation of lithium salt can be realized for the formation of stable SEI at the lithium-SSE interface. Figure 3j is the morphology images based on the surface diagrams of lithium metals after Li–Li cycling with the CPCSE. The lithium metal in the CPCSE cell is flat without obvious dendrite emergence. While in Figure 3k, obvious bulk lithium dendrites indicate the CNCSE has a poor affinity for lithium metal and poor ability to inhibit lithium dendrite during cycling.[21] Hence, the

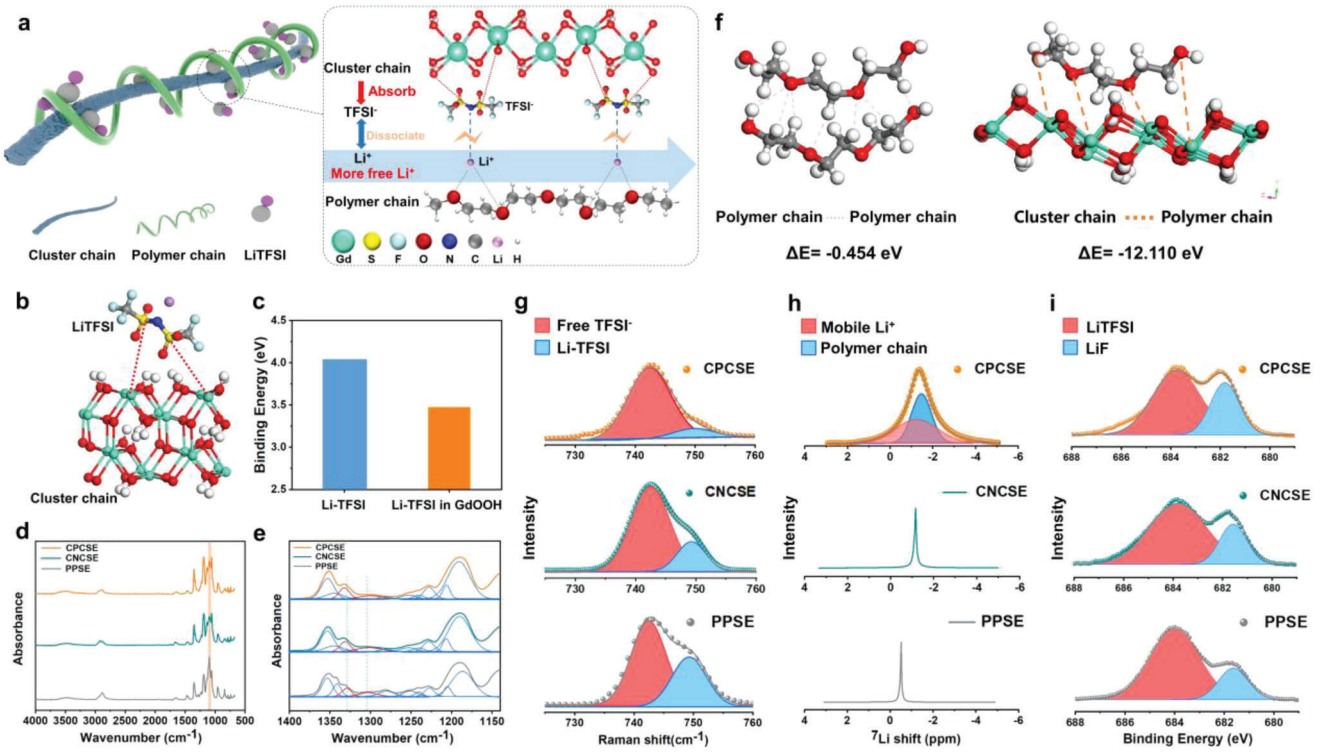

Figure 4. Mechanism analysis of organic–inorganic interface. a) Schematic illustration of the mechanism for enhanced Li-ion transport in organic–inorganic interface. b,c) Calculated Li binding energy of the $TFSI^-$ in lithium salts and adsorbed by the cluster chain surface, LiTFSI (blue), and GdOOH (orange). FTIR spectra of CPCSE, CNCSE, and PPSE at d) 4000–600 cm^{-1} and e) 1400–1140 cm^{-1}. f) Theoretical calculation of adsorption energy between polymer chains, and cluster chain-polymer chain. g) Raman spectra and h) ^7Li solid-NMR of CPCSE, CNCSE, and PPSE. i) XPS spectra of Li metal surface after Li–Li cycling with CPCSE, CNCSE, and PPSE.

effective construction of homogeneous and continuous organic–inorganic chain-adhered interfaces endows SSEs with high ionic conductivity and high interface stability toward Li metal. In-situ optical microscope was conducted to observe the growth of lithium dendrites. The Cu/CSE/Li battery was selected to conveniently observe the edge of lithium dendrites.[22] As shown in Figure S18a–c (Supporting Information), the CPCSE-based system displays a dense and thin Li deposition layer, which proves the successful inhibition of the lithium dendrite growth. In contrast, the CNCSE system leads to obvious protrusions during the growth process of lithium dendrites (Figure S18d–f, Supporting Information). Furthermore, the lithium dendrites in PPSE- based system are thick and uneven, which is unfavorable for maintaining interface stability (Figure S18g–i, Supporting Information).[23] Hence, the effective construction of homogeneous and continuous organic–inorganic chain-adhered interfaces endows SSEs with high interface stability toward Li metal.

It is well-known that the introduction of inorganic materials will lead to the interface effect. The interface effects caused by monodispersed sub-1 nm cluster chains will be discussed in detail. **Figure 4**a illustrates the distribution state of the inorganic cluster chain, organic polymer chains, and LiTFSI in the composite solid-state electrolyte mixture. The surface of the inorganic cluster chains will adsorb $TFSI^-$ anions. Hence, the dissociation degree of the lithium salt will be elevated, and the concentration of mobile Li^+ will increase, constructing the fast Li^+ transport channels. To investigate the interface effect between the cluster chain and the lithium salt, density functional theory (DFT) calculations were carried out to analyze the binding energy between the surface of the cluster chain and the lithium salt in the SSEs. The $TFSI^-$ anions are easy to be attracted by the Lewis-acid site on the inorganic crystal surface (Figure 4b).[17,24] Moreover, the Li^+ binding energy of the $TFSI^-$ anions in lithium salt and absorbed by the surface of cluster chains were calculated (Figure 4c). The lower Li^+ binding energy on the surface of cluster chains means a higher dissociation degree of LiTFSI and more mobile Li^+, indicating the improved Lewis-acid base effect in the homogeneous and continuous interfaces.[25] FT-IR test was performed to investigate the interaction between organic–inorganic interfaces in SSE films. Compared with PEO particles and LiTFSI, the FT-IR spectrum of SSEs has changed after the introduction of inorganic fillers and the formation of films (Figure S19, Supporting Information). As illustrated in Figure 4d, it is evident that at 1300 cm^{-1}, the CSEs exhibit distinct changes for the characteristic peaks of ether oxygen bond compared to the PPSE film, indicating the combination between the polymer chains and inorganic cluster chains.[26] There are seldom characteristic peaks from the residual oleylamine and oleic acid small molecules, which means the residual organic molecules will not affect the interaction between cluster chains and polymer chains. The Lewis acid-base effect between inorganic fillers and lithium salt was also analyzed in Figure 4e. Two red characteristic peaks are

encapsulated as $-SO_2-$ stretching. Compared with the PPSE, the other two CSEs appear peak shifts, indicating the interaction between the surface of inorganic cluster chains and sulfonic acid groups in LiTFSI, which will enhance the dissociation degree of lithium salts, increase the concentration of mobile Li^+, and finally improve the Li^+ transport efficiency.[27] To further investigate the detailed composite states of cluster chains and polymer chains, DFT calculations were employed, and the calculated results show the adsorption energy between polymer chains and cluster chains was much higher than that between two polymer chains (Figure 4f), which means the polymer chains are more easily to be attracted and adsorbed by cluster chains. While inorganic cluster chains possess sub-1 nm diameter and high aspect ratio, it is reasonable to assume the binding sites with polymer chains mainly exhibit 1D distribution. Therefore, the curly polymer chains may be attracted to the surface of cluster chains to be radially aligned and share the same orientation, which could organize into oriented Li^+ fast transport channels. The unique molecular scale ordered state would further improve the transport efficiency of lithium-ions.

To investigate more interface effects after organic–inorganic composite, Raman characterization is performed to study the dissociation state of the lithium salt in the solid-state electrolyte. As shown in Figure 4g, the left side refers to the free $TFSI^-$ anion, and the blue peaks on the right side are undissociated LiTFSI salt. More free $TFSI^-$ anion emerges in the CSEs due to the Lewis acid–base effect.[28] The presence of the highest distribution of free $TFSI^-$ in the CPCSE proves the highest dissociation degree of the lithium salts under the homogeneous and continuous organic–inorganic interface, which will greatly enhance the Li^+ transport efficiency. Solid-state NMR is used to study the distribution of Li-ions in the solid-state electrolytes. The characteristic peak positions of ^7Li in both the solid-state electrolyte with common nanowires and cluster chains are both negatively shifted (Figure 4h), indicating lower interaction around Li-ions.[29] While the characteristic peak of ^7Li in the CPCSE significantly broadens, from which two peaks can be distinguished, the left red peak represents the distribution of mobile Li^+, occupying 50.7%, which mainly exists in the organic–inorganic interface. The peak in blue on the right side represents the Li^+ combined with oxygens of polymer, occupying 49.3%. Therefore, the construction of homogeneous and continuous organic–inorganic interfaces stimulates an increased amount of mobile Li^+, which is beneficial for efficient Li^+ transport.[30] XPS was carried out to detect the side reactions between SSE and lithium metal, Figure 4i shows the characteristic peak spectrum of fluorine element on the lithium metal surface. The peak of the red area on the left is fluorine element in LiTFSI, and blue area on the right represents lithium fluoride generated on the surface of lithium metal.[31] More lithium fluoride content indicates more stable SEI film on the surface of lithium metal. XPS spectrums show that the composition of lithium fluoride on the surface increased obviously after the introduction of cluster chains, and the lithium fluoride produced in the CPCSE shows the highest amount, presenting the generation of the stable SEI film and improved dissociation of lithium salts, which is guided by the strong interactions between uniform and wide range of organic–inorganic interfaces.[32] The experimental results show that the CPCSE creates greater interface stability, which is inseparable from the monodispersion of cluster chains and effective interface construction.

CEI is one of the important components that affect the cathode/SSEs interface. The high-resolution TEM was carried out to investigate the formation of CEI. As shown in **Figure 5**a, an amorphous layer (CEI) was uniformly coated on the surface of CPCSE-based cycled NCM811 particle (NCM-CPCSE). While for NCM-CNCSE and NCM-PPSE particles, the CEI layer is thick and uneven, which will lead to high interfacial resistance at the cathode/SSEs interface (Figure 5b,c). The X-ray photoelectron spectroscopy (XPS) measurement was conducted to characterize the CEI on the cycled NCM811 cathode surface. As shown in Figure 5d–f, the C 1s spectra can be divided into about several peaks, indicating the Li_2CO_3 (C═O) and organic lithium compounds (C–O) in the CEI.[33] The NCM-CPCSE cathode surface contains less organic lithium compounds, indicating less PEO decomposition. Furthermore, the F 1s spectra show the significant content of LiF for stable CEI (Figure 5g-i). The surface of NCM-CPCSE possesses more LiF components, indicating a more stable CEI composition.[34] Therefore, a stable CEI layer can inhibit the decomposition of PEO and maintain a stable cathode/SSE interface. In addition, the CEI on the cycled NCM811 cathode surface was detected by time-of-flight secondary ion mass spectrometry (TOF-SIMS). The C_2HO^- and LiF_2^- anions represent organic lithium compounds and inorganic LiF, respectively. The 3D reconstruction images show the distribution of organic and inorganic components in CEI after cycling with different SSEs (Figure 5j–l). The LiF content in the surface of NCM-CPCSE is the highest, indicating a more stable CEI composition. Therefore, the stable CEI can suppress the further decomposition of PEO, thereby leading to a low content of organic lithium compounds. On the contrary, the NCM-PPSE surface has less LiF and more organic lithium compounds, which means that the unstable CEI layer is difficult to suppress the continuous decomposition of PEO. The distribution of different components can also be seen from the depth profile in Figure 5m,n. This result is consistent with the conclusion of the previous XPS analysis. The monodispersed cluster chains connect to form homogeneous, large-scale, and continuous fully active Li+ conductive networks, which lead to full dissociation of lithium salts. Thus, a stable LiF-rich CEI layer can be constructed to reduce the side reaction of the cathode-SSE interface. Furthermore, a dense and uniform CEI on the NCM-CPCSE surface can also weaken the interface impedance caused by the space charge layer effect.[35] On the contrary, the CEI layer is uneven and shows a continuous growth trend in the control group, making it difficult to relieve the impact of space charge layer between the cathode and SSE. Accelerating rate calorimeter (ARC) was conducted to study the interfacial thermal stability. The onset temperature (Tonset) is the temperature at which side reactions begin to occur inside the cells. As shown in Figure S20 (Supporting Information), the CPCSE-based cell displays higher T_{onset} and longer self-heating time, indicating the stable interface inside the cells. Then, the PPSE-based cell undergoes the first thermal runaway at 242 °C. In contrast, the CPCSE-based cell shows higher thermal runaway temperature (T_{tr}), lower T_{max}, and greatly delays the thermal runaway time. As a result, the CPCSE-based pouch cell presents great interfacial thermal stability, which may benefit by the stable SEI and CEI induced by fully active Li^+ conductive networks.[36]

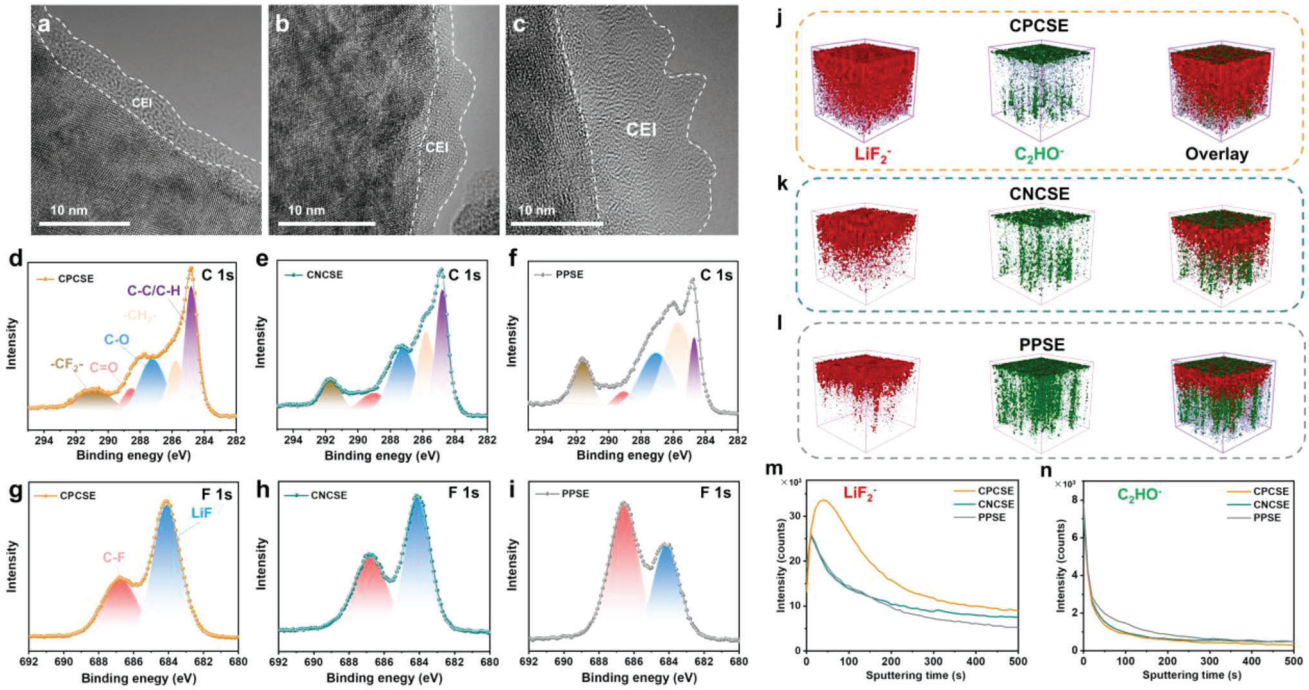

Figure 5. The CEI study for the cycled NCM811 cathode with different SSEs. a–c) High-resolution TEM images of NCM811 particles after solid-state full cell cycling with different SSEs. d–i) XPS spectra about the C 1s and F 1s of the cycled NCM811 cathode. j–l) TOF-SIMS 3D reconstruction of the cycled NCM811 cathode surface. TOF-SIMS depth profiles of m) LiF_2^-, and n) C_2HO^- on the cycled NCM811 cathode surface.

The performance of the SSE was further evaluated with the solid-state full cell. **Figure 6**a shows the inner diagram of the composite cathode material. The CPCSE is introduced into the cathode material as the ionic conductive agent and binder. The efficient Li^+ transport channels composed of cluster chain and polymer chains will adhere to the surface of the cathode material particles to optimize the Li^+ transport path between the cathode particles.[37] The rate performances of solid-state batteries are tested from 0.1 to 2 C (Figure 6b). The capacities of SSLBs based on CPCSE remain stable after the current increasing, and still show a capacity of 121 mAh g^{-1} at 2 C. While the capacities of the control groups decrease significantly with the increase of current, which are below 100 mAh g^{-1} at 2 C. The monodispersion of cluster chains and efficient interface construction of cluster chains/polymer chains provide decreased PEO crystallinity and fully active Li^+ conductive networks for fast Li^+ transport channels, which greatly improves the high current tolerance of the solid-state electrolyte. Charge/discharge plateaus slightly expand and remain stable under increasing current (Figure 6c). However, the polarization of the control groups increases significantly under increasing current, indicating low Li^+ transport efficiency (Figure S21a,b, Supporting Information). Based on the excellent Li^+ transport performance of the CPCSE and optimized Li^+ transport channels in the cathode material, the assembled SSLBs exhibit consistently excellent cycling stability, maintaining high capacity retention of 87.7% after 1000 cycles at 0.5 C (Figure 6d), capacity retention of 80.2% after 700 cycles at 1 C (Figure 6e), 152 mAh g^{-1} after 100 cycles at 0.1 C, respectively (Figure S21c, Supporting Information). The coulombic efficiency of solid-state batteries based on CNCSE and PPSE continuously decreases after a long cycle, which means that there are side reactions between electrode and solid-state electrolyte. As mentioned before, the fully active Li^+ conductive networks can dissociate lithium salts and induce the formation of stable SEI, thereby suppressing side reactions at the electrode/SSE interface and providing high interface stability.[38] Charge/discharge curves of LFP/Li SSLBs after 100 cycles are shown in Figure S21d (Supporting Information), homogeneous and continuous organic–inorganic interface endows more 3D efficient Li^+ transport networks. Hence, the charge/discharge curves of SSLBs with CPCSE show stable plateaus after cycling. To investigate the high voltage stability of SSEs. SSLBs with NCM811 cathode were assembled and tested. Charge/discharge curves under different rates also keep stable contributing to the optimization of composite interface (Figure 6f). On the contrary, the control groups exhibit larger electrochemical polarization and lower cycling capacity due to the poor high voltage tolerance of PEO (Figure S21e,f, Supporting Information). The assembled solid-state batteries with NCM811 cathode maintain stable capacity even at 0.5 C, maintaining 142.8 mAh g^{-1} after 250 cycles (93.7% of capacity retention) (Figure 6g), indicating high voltage stability of the CPCSE. The results show excellent cycling performance compared to other works in Table S1 (Supporting Information). The EIS curves show that the interfacial resistance of the LFP/CPCSE-based full cell is much lower than that of the LFP/PPSE-based full cell before cycling, indicating a better interfacial compatibility of CPCSE with both electrodes (Figure 6h,i). After 100 cycles at 0.5 C, the interfacial resistance of the CPCSE-based full cell keeps stable, while that of the CNCSE-based full cell increases significantly. Hence, the EIS results indicate a more stable

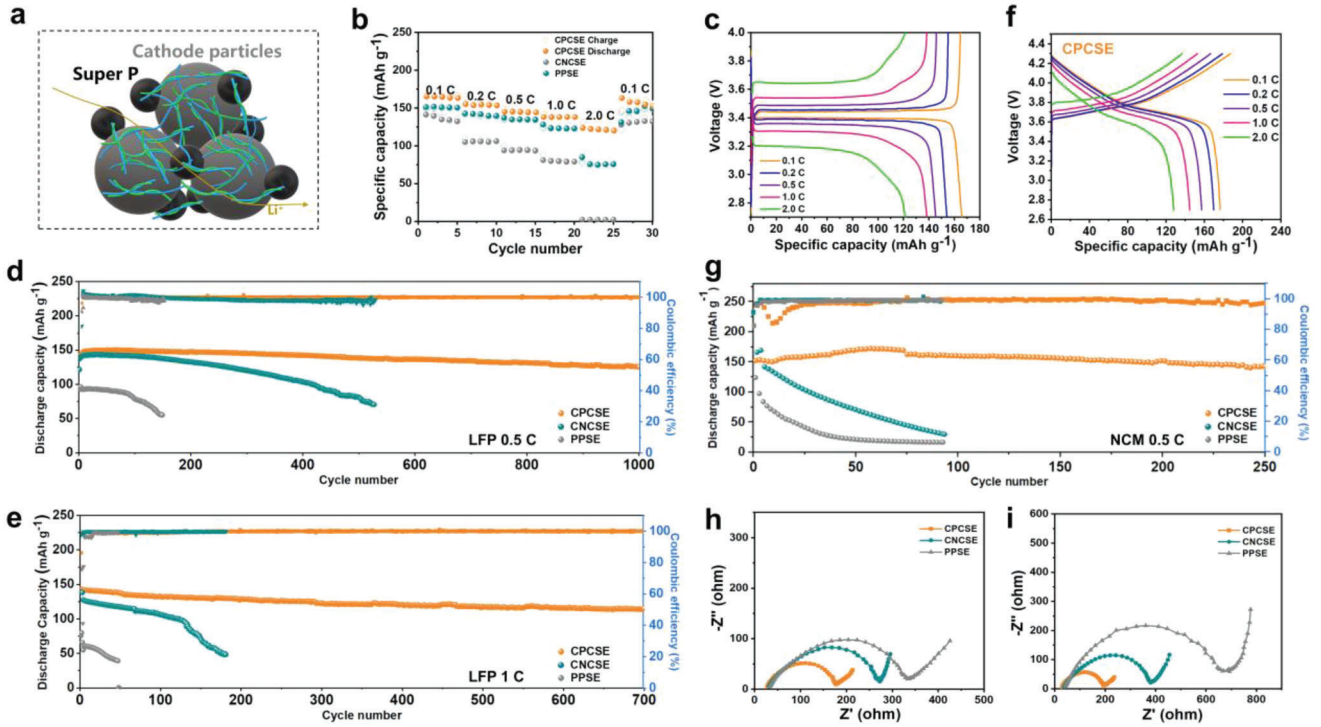

Figure 6. Electrochemical performance of solid-state full cells. a) Schematic illustration of the Li^+ transport channel in the composite cathode. b) Rate performance of the LFP/Li solid-state full cells at different rates. c) Voltage-capacity profiles of LFP/CPCSE/Li solid-state full cells at different current rates. Cycling performance of the LFP/Li solid-state full cells at d) 0.5 C, e) 1 C. f) Voltage-capacity profiles of NCM811/Li solid-state full cells at different current rates. g) Cycling performance of the NCM811/Li solid-state full cells at 0.5 C. The EIS curves of LFP/Li solid-state full cells h) before and i) after 100 cycles.

interface in CPCSE-based full cell due to the lower crystallinity of PEO and fully active Li^+ conductive networks. The fabricated solid punch cell maintains a stable voltage output of 3.4 V (Figure S22a, Supporting Information), and can stabilize the power LED light plate at different bending degrees (Figure S22c,d, S22b-d, Supporting Information), indicating the excellent electrochemical performance and interface stability of the solid-state punch cell. The LFP/CPCSE/Li pouch cell was assembled and kept stable cycling at 0.5 C and 30 °C with a capacity retention of 99% (Figure S22e, Supporting Information), presenting its high practical application value. Compared with other PEO-based composite solid electrolytes with different inorganic fillers, the key performance parameters show huge advantages (Table S2, Supporting Information). This work provides a valuable basis for the organic–inorganic composite solid-state electrolyte. On this basis, we could develop some new polymer materials and compatible solvent systems, and improve the binding state between cluster chains and polymers through surface modification.

3. Conclusion

In summary, a novel type cluster chain/polymer composite solid electrolyte with fully active Li^+ conductive networks was designed and fabricated to enhance Li^+ transport. The sub-1 nm inorganic cluster chains deliver little inner Li^+ non-conductive area and rich exposed surface atoms, which provide more specific interface areas with polymer chains. A compatible SPE and mixed solvent system were designed to achieve monodispersion of sub-1 nm inorganic cluster chains in the polymer matrix, which avoids another kind of Li^+ non-conductive areas caused by agglomeration, constructing homogeneous and continuous Li^+ conductive channels to amplify the interface effects and lead to improved Li^+ transport efficiency. A rational conjecture about the 1D-oriented distribution of organic polymer chains along the inorganic cluster chains is proposed based on the results of the experiments and theoretical calculations. Benefiting from the merits above, the CPCSE possesses high ionic conductivity at room temperature (5.2×10^{-4} S cm^{-1}), high Li^+ transference number (0.62), large distribution of mobile Li^+ (50.7%), and $LiFePO_4$/Li metal and NCM811/Li metal cells with CPCSE deliver excellent electrochemical stability. This research provides a new strategy to break through the current bottleneck in the research field of organic–inorganic composite solid-state electrolytes.

Supporting Information

Supporting Information is available from the Wiley Online Library or from the author.

Acknowledgements

This work was supported by the National Key Research and Development Program of China (2020YFA0715000), National Natural Science Foundation of China (52272234), the Key Research and Development Program

of Hubei Province (2021BAA070), Independent Innovation Projects of the Hubei Longzhong Laboratory (2022ZZ-20), the Sanya Science and Education Innovation Park of Wuhan University of Technology (2021KF0011).

Conflict of Interest

The authors declare no conflict of interest.

Data Availability Statement

The data that support the findings of this study are available from the corresponding author upon reasonable request.

Keywords

inorganic cluster chain, monodispersion, organic–inorganic interface, solid-state lithium batteries, sub-1 nanometer

Received: April 6, 2023
Revised: August 22, 2023
Published online:

[1] a) Y. Guo, S. Wu, Y.-B. He, F. Kang, L. Chen, H. Li, Q.-H. Yang, *eScience.* **2022**, *2*, 138; b) Y. Su, X. Rong, H. Li, X. Huang, L. Chen, B. Liu, Y. S. Hu, *Adv. Mater.* **2022**, *35*, 2209402; c) K. Wen, C. Xin, S. Guan, X. Wu, S. He, C. Xue, S. Liu, Y. Shen, L. Li, C. W. Nan, *Adv. Mater.* **2022**, *34*, 2202143; d) X.-T. Wang, Z.-Y. Gu, E. H. Ang, X.-X. Zhao, X.-L. Wu, Y. Liu, *J. Alloys Compd.* **2022**, *1*, 417.

[2] a) H. Gao, N. S. Grundish, Y. Zhao, A. Zhou, J. B. Goodenough, *Energy Mater. Adv.* **2021**, *2021*, 1932952. b) K. Yoon, S. Lee, K. Oh, K. Kang, *Adv. Mater.* **2022**, *34*, 2104666; c) Y. Zhai, W. Hou, M. Tao, Z. Wang, Z. Chen, Z. Zeng, X. Liang, P. Paoprasert, Y. Yang, N. Hu, S. Song, *Adv. Mater.* **2022**, *34*, 2205560; d) G. Wang, Y. Liang, H. Liu, C. Wang, D. Li, L.-Z. Fan, *J. Alloys Compd.* **2022**, *1*, 434.

[3] a) Q. Guo, F. Xu, L. Shen, S. Deng, Z. Wang, M. Li, X. Yao, *Energy Mater. Adv.* **2022**, b) F. Croce, G. B. Appetecchi, L. Persi, B. Scrosati, *Nature.* **1998**, *394*, 456; c) J. Kang, D. Y. Han, S. Kim, J. Ryu, S. Park, *Adv. Mater.* **2022**, *35*, 2203194; d) J. Ma, G. Zhong, P. Shi, Y. Wei, K. Li, L. Chen, X. Hao, Q. Li, K. Yang, C. Wang, W. Lv, Q.-H. Yang, Y.-B. He, F. Kang, *Environ Sci.* **2022**, *15*, 1503.

[4] a) S. Liu, W. Liu, D. Ba, Y. Zhao, Y. Ye, Y. Li, J. Liu, *Adv. Mater.* **2022**, *35*, 2110423; b) J. Han, M. J. Lee, K. Lee, Y. J. Lee, S. H. Kwon, J. H. Min, E. Lee, W. Lee, S. W. Lee, B. J. Kim, *Adv. Mater.* **2022**, *35*, 2205194; c) S. Y. Kim, J. Li, *Energy Mater. Adv.* **2021**, *2021*, 1519569.

[5] C. Hu, Y. Shen, M. Shen, X. Liu, H. Chen, C. Liu, T. Kang, F. Jin, L. Li, J. Li, Y. Li, N. Zhao, X. Guo, W. Lu, B. Hu, L. Chen, *J. Am. Chem. Soc.* **2020**, *142*, 18035.

[6] J. Cheng, G. Hou, Q. Sun, Z. Liang, X. Xu, J. Guo, L. Dai, D. Li, X. Nie, Z. Zeng, P. Si, L. Ci, *Solid State Ionics* **2020**, *345*, 115156.

[7] a) C. Ma, K. Dai, H. Hou, X. Ji, L. Chen, D. G. Ivey, W. Wei, *Adv. Sci.* **2018**, *5*, 1700996; b) Z. Li, F. Liu, S. Chen, F. Zhai, Y. Li, Y. Feng, W. Feng, *Nano Energy* **2021**, *82*, 105698.

[8] W. Liu, N. Liu, J. Sun, P. C. Hsu, Y. Li, H. W. Lee, Y. Cui, *Nano Lett.* **2015**, *15*, 2740.

[9] a) M. Zhang, P. Pan, Z. Cheng, J. Mao, L. Jiang, C. Ni, S. Park, K. Deng, Y. Hu, K. K. Fu, *Nano Lett.* **2021**, *21*, 7070; b) L. Mai, X. Tian, X. Xu, L. Chang, L. Xu, *Chem. Rev.* **2014**, *114*, 11828; c) Z. Wan, D. Lei, W. Yang, C. Liu, K. Shi, X. Hao, L. Shen, W. Lv, B. Li, Q.-H. Yang, F. Kang, Y.-B. He, *Adv. Funct. Mater.* **2019**, *29*, 1805301.

[10] a) S. Zhang, H. Lin, H. Yang, B. Ni, H. Li, X. Wang, *Adv. Funct. Mater.* **2019**, *29*, 1903477; b) S. Zhang, H. Shi, J. Tang, W. Shi, Z.-S. Wu, X. Wang, *Sci. China Mater.* **2021**, *64*, 2949.

[11] J. Liu, Y. Li, Z. Chen, N. Liu, L. Zheng, W. Shi, X. Wang, *J. Am. Chem. Soc.* **2022**, *144*, 23191.

[12] J. Park, K. An, Y. Hwang, J.-G. Park, H.-J. Noh, J.-Y. Kim, J.-H. Park, N.-M. Hwang, T. Hyeon, *Nat. Mater.* **2004**, *3*, 891.

[13] a) A. B. Rudine, M. G. Walter, C. C. Wamser, *J. Org. Chem.* **2010**, *75*, 4292; b) G. Jiang, O. Erdem, R. Hübner, M. Georgi, W. Wei, X. Fan, J. Wang, H. V. Demir, N. Gaponik, *Nano Res.* **2020**, *14*, 1078.

[14] C.-C. Li, C.-L. Huang, *Colloid. Surface A* **2010**, *353*, 52.

[15] S. Hu, H. Liu, P. Wang, X. Wang, *J. Am. Chem. Soc.* **2013**, *135*, 11115.

[16] H. Liu, Q. Gong, Y. Yue, L. Guo, X. Wang, *J. Am. Chem. Soc.* **2017**, *139*, 8579.

[17] a) N. Wu, P.-H. Chien, Y. Qian, Y. Li, H. Xu, N. S. Grundish, B. Xu, H. Jin, Y.-Y. Hu, G. Yu, J. B. Goodenough, *Angew. Chem., Int. Ed.* **2020**, *59*, 4131; b) G. B. Appetecchi, F. Croce, L. Persi, F. Ronci, B. Scrosati, *Electrochim. Acta.* **2000**, *45*, 1481.

[18] a) X. Wang, K. Guo, Y. Xia, Y. Min, Q. Xu, *ACS Appl. Mater. Interfaces.* **2021**, *13*, 60907; b) F. Liu, Y. Cheng, X. Zuo, R. Chen, J. Zhang, L. Mai, L. Xu, *Chem. Eng. J.* **2022**, *441*, 136077.

[19] a) K. Pan, L. Zhang, W. Qian, X. Wu, K. Dong, H. Zhang, S. Zhang, *Adv. Mater.* **2020**, *32*, 2000399; b) W. Zha, F. Chen, D. Yang, Q. Shen, L. Zhang, *J. Power Sources.* **2018**, *397*, 87.

[20] a) A. J. Bhattacharyya, J. Maier, *Adv. Mater.* **2004**, *16*, 811; b) H. Yamada, A. J. Bhattacharyya, J. Maier, *Adv. Funct. Mater.* **2006**, *16*, 525.

[21] Z. Wang, L. Shen, S. Deng, P. Cui, X. Yao, *Adv. Mater.* **2021**, *33*, 2100353.

[22] H. Qiu, T. Tang, M. Asif, X. Huang, Y. Hou, *Adv. Funct. Mater.* **2019**, *29*, 1808468.

[23] Z. Ning, D. S. Jolly, G. Li, R. De Meyere, S. D. Pu, Y. Chen, J. Kasemchainan, J. Ihli, C. Gong, B. Liu, D. L. R. Melvin, A. Bonnin, O. Magdysyuk, P. Adamson, G. O. Hartley, C. W. Monroe, T. J. Marrow, P. G. Bruce, *Nat. Mater.* **2021**, *20*, 1121.

[24] H. Xu, P.-H. Chien, J. Shi, Y. Li, N. Wu, Y. Liu, Y.-Y. Hu, J. B. Goodenough, *Proc. Natl. Acad. Sci. USA.* **2019**, *116*, 18815.

[25] X. Ao, X. Wang, J. Tan, S. Zhang, C. Su, L. Dong, M. Tang, Z. Wang, B. Tian, H. Wang, *Nano Energy.* **2021**, *79*, 105475.

[26] H. Chen, D. Adekoya, L. Hencz, J. Ma, S. Chen, C. Yan, H. Zhao, G. Cui, S. Zhang, *Adv. Energy Mater.* **2020**, *10*, 2000049.

[27] O. Sheng, C. Jin, J. Luo, H. Yuan, H. Huang, Y. Gan, J. Zhang, Y. Xia, C. Liang, W. Zhang, X. Tao, *Nano Lett.* **2018**, *18*, 3104.

[28] L. Wang, Y. Zhong, Z. Wen, C. Li, J. Zhao, M. Ge, P. Zhou, Y. Zhang, Y. Tang, G. Hong, *Sci. China Mater.* **2022**, *65*, 2179.

[29] S. Xu, Z. Sun, C. Sun, F. Li, K. Chen, Z. Zhang, G. Hou, H. M. Cheng, F. Li, *Adv. Funct. Mater.* **2020**, *30*, 2007172.

[30] J. Zheng, M. Tang, Y. Y. Hu, *Angew. Chem. Int. Ed. Engl.* **2016**, *55*, 12538.

[31] Z. Zhang, Y. Huang, G. Zhang, L. Chao, *Energy Storage Mater.* **2021**, *41*, 631.

[32] a) Y. Liu, R. Hu, D. Zhang, J. Liu, F. Liu, J. Cui, Z. Lin, J. Wu, M. Zhu, *Adv. Mater.* **2021**, *33*, 2004711; b) H. Xu, C. Sun, S. Zhang, H. Zhang, Z. Liu, Y. Tang, G. Cui, *ChemSusChem* **2023**, *16*, 202202334.

[33] B. Wen, Z. Deng, P.-C. Tsai, Z. W. Lebens-Higgins, L. F. J. Piper, S. P. Ong, Y.-M. Chiang, *Nat. Energy.* **2020**, *5*, 578.

[34] a) X. Yang, M. Jiang, X. Gao, D. Bao, Q. Sun, N. Holmes, H. Duan, S. Mukherjee, K. Adair, C. Zhao, J. Liang, W. Li, J. Li, Y. Liu, H. Huang, L. Zhang, S. Lu, Q. Lu, R. Li, C. V. Singh, X. Sun, *Environ Sci.* **2020**, *13*, 1318; b) X. Tang, X. Xu, M. Bai, M. Zhang, H. Wang, Z. Wang, A. Shao, H. Wang, Y. Ma, *Adv. Funct. Mater.* **2022**, *33*, 2210465.

[35] J. Haruyama, K. Sodeyama, L. Han, K. Takada, Y. Tateyama, *Chem. Mater.* **2014**, *26*, 4248.

[36] a) R. Chen, A. M. Nolan, J. Lu, J. Wang, X. Yu, Y. Mo, L. Chen, X. Huang, H. Li, *Joule.* **2020**, *4*, 812; b) X. Zhang, L. Huang, B. Xie, S. Zhang, Z. Jiang, G. Xu, J. Li, G. Cui, *Adv. Energy Mater.* **2023**, *13*, 2203648; c) Y. Zhang, L. Yu, X.-D. Zhang, Y.-H. Wang, C. Yang, X. Liu, W.-P. Wang, Y. Zhang, X.-T. Li, G. Li, S. Xin, Y.-G. Guo, C. Bai, *Sci. Adv.* **2023**, *9*, eade5802.

[37] Y. Cheng, J. Shu, L. Xu, Y. Xia, L. Du, G. Zhang, L. Mai, *Adv. Energy Mater.* **2021**, *11*, 2100026.

[38] S. Ko, T. Obukata, T. Shimada, N. Takenaka, M. Nakayama, A. Yamada, Y. Yamada, *Nat. Energy.* **2022**, *7*, 1217.